

Zfp217 mediates m⁶A mRNA methylation to orchestrate transcriptional and post-transcriptional regulation to promote adipogenic differentiation

Tongxing Song^{1,2,†}, Yang Yang^{1,2,†}, Hongkui Wei^{1,2}, Xiaowei Xie^{1,2}, Jinxin Lu^{1,2}, Qianhui Zeng^{2,3}, Jie Peng^{1,2}, Yuanfei Zhou^{1,2}, Siwen Jiang^{2,3,*} and Jian Peng^{1,2,*}

¹Department of Animal Nutrition and Feed Science, College of Animal Science and Technology, Huazhong Agricultural University, Wuhan 430070, China, ²The Cooperative Innovation Center for Sustainable Pig Production, Wuhan 430070, China and ³Key Laboratory of Animal Genetics, Breeding and Reproduction Ministry of Education, College of Animal Science and Technology, Huazhong Agricultural University, Wuhan 430070, China

Received September 28, 2018; Revised April 14, 2019; Editorial Decision April 16, 2019; Accepted April 28, 2019

ABSTRACT

A complex and highly orchestrated gene expression program chiefly establishes the properties that define the adipocyte phenotype, in which the vast majority of factors are involved in transcriptional regulation. However, the mechanisms by post-transcriptional modulation are poorly understood. Here, we showed that zinc finger protein (Zfp217) couples gene transcription to m⁶A mRNA modification to facilitate adipogenesis. Zfp217 modulates m⁶A mRNA methylation by activating the transcription of m⁶A demethylase FTO. Consistently, depletion of *Zfp217* compromises adipogenic differentiation of 3T3L1 cells and results in a global increase of m⁶A modification. Moreover, the interaction of Zfp217 with YTHDF2 is critical for allowing FTO to maintain its interaction with m⁶A sites on various mRNAs, as loss of Zfp217 leads to FTO decrease and augmented m⁶A levels. These findings highlight a role for Zfp217-dependent m⁶A modification to coordinate transcriptional and post-transcriptional regulation and thus promote adipogenic differentiation.

INTRODUCTION

The global incidence of obesity and Type 2 diabetes has increased over the last three decades. It is well confirmed that adipose tissue greatly contributes to obesity-associated diseases. Thus, the manipulation of adipocyte differentiation and maturation could be a promising strategy for the treatment of obesity-related diseases (1). Considerable efforts have been made to elucidate the role of transcriptional

and epigenetic regulation in adipogenesis and identify a vast majority of key regulators and pathways (1,2). However, the function of post-transcriptional regulation in adipogenesis is not well understood.

N⁶-methyladenosine (m⁶A) has been identified as the most abundant modification present on eukaryotic messenger RNA (mRNA) (3–5), and plays a role in regulating cell fate and lineage transition in embryonic stem cells (5–8). The ‘writer’ complex, which catalyzes m⁶A mRNA methylation consists of methyltransferase-like 3 (METTL3), methyltransferase-like 14 (METTL14) and Wilms tumor 1-associated protein (WTAP), was recently shown to regulate mitotic clonal expansion in adipogenesis (9,10). Notably, the first ‘eraser’ protein mediating the reversal of m⁶A methylation, fat mass and obesity-associated protein (FTO) has been identified in Genome-Wide Association Studies as a candidate in obesity (11,12) and also plays a critical role in maintaining adipogenesis through RNA splicing in an m⁶A-dependent way (13–15). Recently, it was reported that the m⁶A-binding protein YTH domain-containing family 2 (YTHDF2), in addition to acting as a reader of m⁶A modifications, can also prevent FTO from demethylating heat shock stress-induced transcripts (3–5,16). However, the regulation of m⁶A modification by proteins in adipogenesis is poorly understood.

Zinc finger protein 217 (Zfp217, human homolog ZNF217) is a well-known oncogenic protein upregulated in a variety of human tumors (17–19), and is also critical for embryonic stem cell differentiation (8,20,21). Noticeably, Zfp217 tightly couples gene transcription with m⁶A modification on the nascent RNA, suggesting a key role for Zfp217 in coordinating epigenetic and epitranscriptomic networks (8,22). While we previously identified a novel role for Zfp217 in adipogenesis, a detailed Zfp217-dependent

*To whom correspondence should be addressed. Tel: +86 027 8720122; Email: pengjian@mail.hzau.edu.cn
Correspondence may also be addressed to Siwen Jiang. Tel: +86 027 8720122; Email: jiangsiwen@mail.hzau.edu.cn
†The authors wish it to be known that, in their opinion, the first two authors should be regarded as Joint First Authors.

mechanism has not been well characterized (23,24). However, these studies raise the possibility that Zfp217 may modulate the m⁶A modification to accelerate adipogenesis.

In this study, we find that *Zfp217* deficiency impairs adipogenesis in 3T3L1 cells and leads to a global increase in m⁶A mRNA methylation. Furthermore, Zfp217 transcriptionally activates *FTO* gene expression and orchestrates m⁶A mRNA modification in an m⁶A-YTHDF2-dependent manner. Taken together, these findings illustrate that Zfp217 is an essential and multi-faceted regulator that promotes adipogenesis at both the transcriptional and post-transcriptional level.

MATERIALS AND METHODS

Cell culture and differentiation

3T3L1 and HEK293T cells were cultured in Dulbecco's modified Eagle's medium (Gibco, San Diego, CA, USA) with 10% fetal bovine serum (FBS, Gibco) and 1% penicillin/streptomycin. MEFs were prepared from 13.5-d embryos from *Zfp217*^{+/-} × *Zfp217*^{+/-} mice as reported elsewhere (25). For adipogenic differentiation, cells were treated with 1 μM DEX, 0.5 mM isobutyl-methylxanthine, 10 μg/ml insulin and 100 μmol/l Indomethacin. After 2 days, the cells were transferred to 10% FBS medium containing only 10 μg/ml insulin and maintained in this medium for 2 days; subsequently, cells were maintained in 10% FBS for another 2 days.

CRISPR/Cas9 knockout of Zfp217

The *Zfp217* gene sequence was entered into the Zhang Lab's online generator (<http://crispr.mit.edu/>), and the three CRISPR guide sequences that bind upstream and downstream with close proximity to target (TAG = 0) were chosen. Guide RNA (sgRNA) sequences were listed in Supplementary Table S1. These sequences were cloned into the pSpCas9(BB)-2A-GFP (PX458) plasmid (Addgene Plasmid # 48138). The activity of these sgRNAs was analyzed by T7E1 assay and those with the highest activity were chosen for further use. To establish *Zfp217* knockout 3T3L1 cell line, PX458-sgZfp217 was transfected into 3T3L1 cells using Lipofectamine 2000. Two days after transfection, single cell-derived clone was sorted with fluorescence-activated of eGFP⁺ using a BD FACSAria II sorter- 488 nm (100 mw) (BD Biosciences, San Jose, CA, USA). After 7–10 days for expansion, clones were screened for CRISPR-mediated deletion with sanger sequencing. *Zfp217* knockout mice got from Cyagen Biosciences Inc. (China) and animal procedures were performed under the ethical guidelines of the Institutional Animal Care and Use Committees at the Huazhong Agricultural University.

Plasmids and transfection

Zfp217, *YTHDF2* and *FTO* cDNA was obtained from a mouse cDNA library and cloned into a pCMV-N-FLAG vector (Clontech, Pato Alto, CA, USA) at the BamHI sites. About 2000 bp of *FTO* promoter fragments were cloned into a pGL3-basic vector (Promega, Madison, USA) at the KpnI and XhoI sites. Deletion fragments of Zfp217-binding

site (ATTCTG) were generated using this plasmid DNA as a template. The primers used for PCR amplification are listed in Supplementary Table S2. For transfection, cells were seeded into a 12-well plate and transfected with plasmids using Lipofectamine 2000 (Invitrogen, Carlsbad, CA, USA), following the manufacturer's instructions.

Oil red O (ORO) staining

The cells were washed twice with phosphate-buffered saline (PBS) and fixed in 4% paraformaldehyde for 30 min at room temperature. Cells were then washed again with PBS and stained with freshly diluted Oil red O (Sigma-Aldrich, St. Louis, MO, USA) for 15 min. After staining, the cells were washed with PBS and photographed using a microscope (Nikon, Japan).

RNA isolation, real-time quantitative PCR (QPCR) and m⁶A dot blot

Total RNA was extracted using the Trizol reagent (Invitrogen, USA) and transcribed into cDNA using a first-strand cDNA synthesis kit (TOYOBO, Japan). Quantitation of the mRNA level by QPCR was performed on a real-time PCR system using iTaq Universal SYBR Green Supermix (Bio-Rad, Richmond, CA, USA). The cycle thresholds (C_T) of the target gene was normalized to the C_T of the internal reference *β-actin* gene using the formula ' $2^{-\Delta\Delta C_T}$ ', which yielded relative gene expression level values. The primers used are listed in Supplementary Table S3. For m⁶A dot blots, RNA samples were denatured at 65°C for 5 min. An equal volume of chilled 20× SSC buffer (Sigma-Aldrich) was then added before samples were spotted on the Amersham Hybond-N⁺ membrane (GE Healthcare). After UV crosslinking, the membrane was washed with PBST buffer, blocked with 5% non-fat milk and incubated with anti-m⁶A antibody (Abcam, USA, #151230) overnight at 4°C. Then, the secondary antibody was incubated at room temperature for 1 h. The membrane was exposed by using Western-Bright™ Peroxide (Advansta, California, USA) in the imaging system (Carestream, New York, USA).

Western blot and immunoprecipitation (IP)

The cells were extracted with protein lysis buffer (Beyotime, China) supplemented with protease inhibitor cocktail. Protein concentration was determined using the BCA Kit (Beyotime, China). Proteins (25–35 μg) were separated on a 10% polyacrylamide precast SDS gel (Bio-Rad) followed by blotting on PVDF membranes (Millipore Billerica, MA, USA). The membranes were probed with the following antibodies against: Zfp217 (Abcam, USA, #48133), METTL3 (Abcam, #195352), ALKBH5 (Abcam, #69325), PPARγ (Cell Signaling Technology, USA, #C26H12), aP2 (Cell Signaling Technology, #D25B3), FTO (Santa cruz, USA, #sc-271713), YTHDF2 (Proteintech, China, #24744-1-AP), β-actin (Abclonal, China, #AC026), LMNB1 (Abclonal, #A1910) and Tublin (Abclonal, #AC021). Secondary antibodies and detection were according to description previously. For IP experiments, cells were lysed in IP

buffer (Beyotime, China) and incubated with antibodies followed by the pull-down with protein A/G beads for subsequent western blot analysis.

Cell cycle and apoptosis analysis

For cell cycle analysis, cells were trypsinized and fixed with 70% ethanol. and then incubated with 50 $\mu\text{g/ml}$ propidium iodide (PI). DNA content of single cell was quantified by flow cytometry analysis. For cell apoptosis analysis, cells were trypsinized and incubated with Annexin V-PE/7-AAD. Dead cells were quantified by flow cytometry analysis.

Luciferase reporter assays

Luciferase reporter assays were performed as described in a previous study (26). The *FTO*-promoter (or *Zfp217* binding site-deleted fragments) luciferase vector and renilla luciferase-expressing plasmid (pTK) were co-transfected with pCMV-N-Flag-*Zfp217* or empty vector. After 24 h transfection, cells were lysed using Dual-Glo luciferase reagent (Promega, Madison, USA). The luciferase activity was determined using a dual-luciferase reporter assay system and luminometer (Dynex Technologies, UK). The luciferase values were normalized to the renilla values.

Chromatin immunoprecipitation (ChIP) assay

ChIP was performed using the ChIP Assay Kit according to the manufacturer's instructions (Beyotime, China). Briefly, after crosslinking (1% formaldehyde), cells were quenched by addition of 0.125 M glycine and harvested in SDS lysis buffer for sonication digestion, the DNA-protein complexes were immunoprecipitated with ChIP grade antibodies against *Zfp217* or IgG. DNA obtained from the immunoprecipitation were analyzed by quantitative PCR and normalized to inputs. The primers used are listed in Supplementary Table S4.

Cytoplasmic and nuclear extracts extraction

Cytoplasmic and nuclear extracts were prepared using nuclear and cytoplasmic extraction kit (BestBio, China) according to the manufacturer's instructions. The protein expression level of *Zfp217* and *YTHDF2* in nucleus or cytoplasm were detected by western blot. Lamin B1 was used as a nuclear envelope marker. Tubulin was used as a cytoplasmic protein marker.

Immunofluorescence and confocal imaging

Cells were washed twice with PBS and fixed in 4% paraformaldehyde for 30 min at room temperature. After blocked with 1% BSA for 1 h. Cells were stained with indicated primary antibody *Zfp217* (Thermo fisher, #MA5-27088) and *YTHDF2* (Proteintech, #24744-1-AP) 2 h, followed by incubation with Alexa Fluor 555 goat anti-mouse secondary antibody or Alexa Fluor 488 goat anti-rabbit secondary antibody for 1 h. DAPI (4,6-diamidino-2-phenylindole; Molecular Probes) was used to label DNA.

Confocal imaging performed using a confocal laser scanning microscope (Carl Zeiss, Germany) equipped with an incubation chamber and a motorized table.

RNA interference

Synthetic siRNA oligonucleotides specific for regions in the mouse *Zfp217* and *YTHDF2* mRNA were designed and synthesized by GenePharma (Shanghai, China). The sequences that gave successful knockdown were *Zfp217*-1, 5'-CACACTTCCACGGAATCATAC-3'; *Zfp217*-2, 5'-TCACATCAGCACCTATCTAAC-3' (8); *METTL3*, 5'-CGTCAGTATCTTGGGCAAATT-3' (8) *YTHDF2*, 5'-GCTCCAGGCATG AATACTATA -3'(16); *Ccdc141*, 5'-GCGCAUCACUUUCA GACAATT-3'; *Hspa1a-1*, 5'-GCGACCUGAACAAAGAGCAUTT -3'; *Hspa1a-2*, 5'-GACUUCUA CACAUCAUCATT -3'; *Efcab11*, 5'-CCCAACACUUCUGGUGU UUTT -3'. Negative control (NC) siRNA was 5'-TTCTCCGAACGTGTCACGT-3'. Cells were transfected at 50–70% confluence with siRNA duplexes using Lipofectamine RNAiMAX (Invitrogen) in accordance with the manufacturer's instructions.

Quantitative analysis of m⁶A level using LC-MS/MS

Quantification of the m⁶A and cap m⁶Am in polyadenylated RNA using LC-MS/MS as described previously (27–29). Polyadenylated RNA was purified from total RNA using Dynabeads® mRNA DIRECT kit (ThermoFisher, #61006) according to the manufacturer's instructions, and further treated with RppH (NEB, M0356S) to remove the cap. About 200 ng polyadenylated RNA was digested with 2U nuclease P1 (Sigma-Aldrich, St. Louis, MO, USA) at 37°C for 2 h in 25 μl of buffer containing 25 mM NaCl and 2.5 mM of ZnCl₂, followed by the addition of NH₄HCO₃ (1 M, 3 μl) and alkaline phosphatase (0.5 U) for 2 h at 37°C. The digestion mixture was diluted to 1 ml using deionized water and centrifuged at 10 000 rpm for 5 min to remove any solid material. The digestion mixture was then filtered with 0.22 μm Millipore membrane and 5 μl of this solution was injected into the LC-MS/MS system. A, m⁶A and m⁶Am were later separated by UPLC-ESI-QQQ on a C18 column (Rapid Resolution HT, 50 mm \times 2.1 mm I.D, 1.8 μm , Agilent, Santa Clara, California, USA). Formic acid in water (0.1%, v/v, solvent A) and formic acid in methanol (0.1%, v/v, solvent B) were employed as the mobile phase. The mass spectrometry detection was performed under positive electrospray ionization mode, by which the product ion scans of the protonated A at m/z (268 \rightarrow 136), m⁶A at m/z (282 \rightarrow 150) and m⁶Am m/z (296 \rightarrow 150) were acquired. The quantification was carried out using a standard curve generated from A, m⁶A and m⁶Am standards (0.1–10 nM for m⁶A and m⁶Am, 50–2000 nM for A) ran during the same batch of the samples. The m⁶A and m⁶Am levels were calculated as the ratio of m⁶A and m⁶Am to A.

MeRIP QPCR of target genes

m⁶A immunoprecipitation (MeRIP) was performed as described previously (27,30,31). A 1 μg aliquot of m⁶A antibody (Abcam, #ab151230) and Normal rabbit IgG (AB-

clonal, #AC005) were respectively conjugated to 20 μ l SureBeads protein A/G mixed magnetic beads (Bio-rad, #161-4013; #161-4023) overnight at 4°C. A 100 μ g aliquot of fragmented total RNA was incubated with the antibody in immunoprecipitation buffer (50 mM Tris-HCl, 750 mM NaCl and 0.5% NP40) supplemented with 40U RNase inhibitor overnight at 4°C. RNA was eluted from the beads by incubation in 300 μ l of elution buffer (5 mM Tris-HCl, 1 mM EDTA and 0.05% SDS) with 8.4 μ g of proteinase K for 1.5 h at 50°C. Following phenol extraction and ethanol precipitation, the input and m⁶A-enriched RNA were reversely transcribed with random hexamers, and the enrichment was determined by QPCR. The primers used for detection for m⁶A-enriched gene mRNA were shown in Supplementary Table S5.

***In vitro* RNA pull-down and competition assay**

Synthesized mRNA with a single m⁶A at A103 was labeled by biotin (Takara, Japan). Binding of the labeled RNA to streptavidin magnetic beads was performed in RNA capture buffer (20 mM Tris, pH 7.5, 1 M NaCl, 1 mM EDTA) for 30 min at room temperature with rotation. The RNA-protein binding reaction was conducted in protein-RNA binding buffer (20 mM Tris (pH 7.5), 50 M NaCl, 2 mM MgCl₂, 0.1% Tween-20 Detergent) at 4°C for 60 min with rotation. After washing three times with the wash buffer (20 mM Tris (pH 7.5), 10 mM NaCl, 0.1% Tween-20 Detergent), protein was eluted by Biotin Elution Buffer (Pierce) and detected by western blot (16,32). *In vitro* competition assay was performed as previous report (29). Briefly, 1 μ g polyadenylated RNA purified from 3T3L1 cells was incubated with 2 μ g FTO, Zfp217 and YTHDF2 in 100 μ l of reaction buffer containing KCl (100 mM), MgCl₂ (2 mM), SUPERNase In (0.2 U/ml), L-ascorbic acid (2 mM), α -ketoglutarate (300 mM), (NH₄)₂Fe(SO₄)₂·6H₂O (150 mM) and 50 mM of HEPES buffer (pH 6.5). The reaction buffer was incubated for 3 h at room temperature, and quenched by adding 5 mM EDTA. RNA was isolated by TRIzol and followed by dot blot.

Localized surface plasmon resonance (LSPR)

The protein-protein and protein-RNA interactions were measured using an OpenSPR localized surface plasmon resonance (LSPR) biosensor (Nicoya Life Science, Inc., Kitchener, Canada), as described previously (33,34). In brief, 100 μ l (1 μ g/ μ l) of Flag-YTHDF2 was immobilized on a COOH sensor chip (Nicoya # SEN-AU-100-12-COOH) at a flow rate of 20 μ l/min in 1 \times PBS buffer (pH = 7.4, RNase-free) and 0.1% v/v Tween 20. Free activated carboxyl groups were deactivated with the addition of 100 μ l blocking buffer (Nicoya). The immobilized protein was washed with running buffer (1 \times PBS, pH 7.4; 0.1% v/v Tween 20; 0.1% w/v BSA, RNase-free) until a stable baseline was achieved. Buffer-matched recombinant Flag-Zfp217 (20 μ l; 325–650 nM) or m⁶A-modified mRNA were injected into the flow cell at a rate of 20 μ l/min. Following a 5-min interaction time, the dissociation was recorded for an additional 7 min. Kinetic binding analysis was performed with the TraceDrawer software package (Ridgeview Instruments, Uppsala, Sweden).

RNA-seq and relative data analysis

RNA-Seq was performed at Novogene Bioinformatics Institute (China). In brief, RNA samples from WT and Zfp217 knockout with MDI inducing 0 and 2 d were extracted using the Trizol reagent (Invitrogen). RNA purity was checked using the NanoPhotometer[®] spectrophotometer (IMPLEN, CA, USA). Sequencing libraries were generated using NEBNext[®] Ultra[™] RNA Library Prep Kit for Illumina[®] (NEB, USA). Sequencing was then performed on an Illumina HiSeq platform and 150 bp paired-end reads were generated. Reads of each sample were aligned to the mouse genome (NCBI build 38/mm10) using Bowtie v2.2.3. HTSeq v0.6.1 was used to count the reads numbers mapped to each gene and then FPKM of each gene was calculated. Differential expression genes was identified by the DESeq R package (1.18.0) using a false discovery rate (FDR) < 0.05 and fold-change > 1.5 or < 0.7. Gene Ontology (GO) enrichment analysis of differentially expressed genes was implemented by the Goseq R package.

m⁶A-seq assays and data analysis

RNA samples were fragmented by RNA fragmentation buffer (10 mM Tris-HCl (pH 7.0), 10 mM ZnCl₂). Fragmented RNA was incubated for 2 h at 4°C with 0.5 mg/ml anti-m⁶A antibody in IP buffer (150 mM NaCl, 0.1% Igepal CA-630, 10 mM Tris-HCl (pH 7.4)) with RNasin (40 U/ μ l). Library preparation and sequencing were performed at Novogene Bioinformatics Institute (China) as previously description. For data analysis, read sequences were filtered by the FASTQC and then aligned to the mouse genome (NCBI build 38/mm10) using BWA mem v 0.7.12. MACS version 2.1.0 was used for peak detection. A *q*-value threshold of enrichment of 0.05 was used for all data sets. MEME and DREME were used to detect the sequence motif, after which, Tomtom software was performed to annotate the motifs. Integrative Genomics Viewer (IGV) were used to visualize the distributions of the m⁶A peaks.

Statistical analysis

Data were analyzed using GLM procedures followed by Tukey's post-hoc tests using the SAS statistical package (v 8.2, SAS Inst., Inc., Cary, NC). All values are presented as mean \pm standard deviation. *P* value < 0.05 indicated significant difference.

RESULTS

Loss of Zfp217 retards adipose differentiation

To explore the role of Zfp217 in adipogenic differentiation, we conducted loss-of-function assays by using siRNA that exhibited significant reduction of Zfp217 mRNA and protein (Figure 1A and Supplementary Figure S1). Zfp217 knockdown significantly blocked adipogenesis as indicated by decreased level of Oil Red O staining as well as lower expression of key adipogenic genes PPAR γ , aP2, LPL and Adiponectin (Figure 1B–D). Furthermore, Zfp217 gene was totally deleted using CRISPR/Cas9 system (Figure 1E), which abolished adipogenesis in 3T3L1 cells (Figure

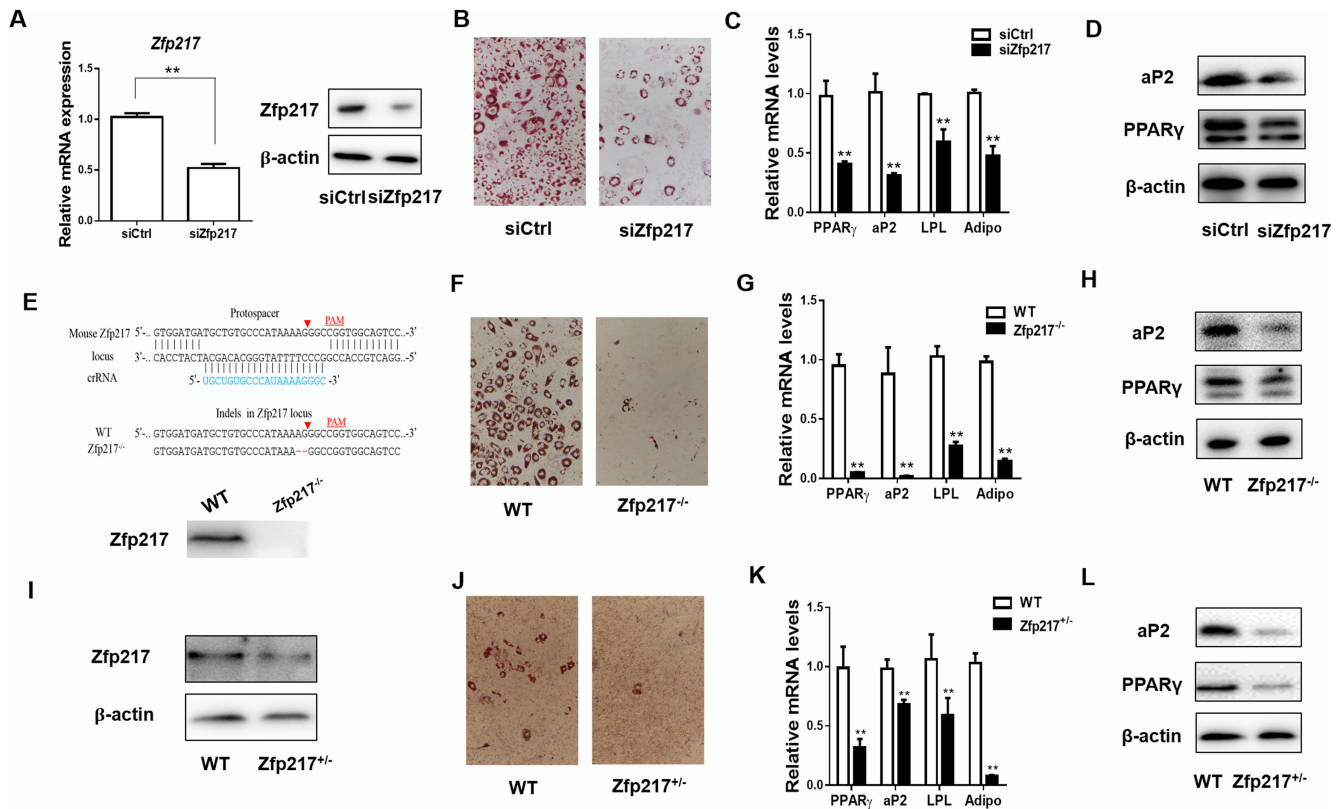


Figure 1. Zfp217 depletion impairs adipogenesis of 3T3L1 cells. (A) The mRNA and protein expression levels of Zfp217 were detected in 3T3L1 cells treated with siRNA for 36 h ($n = 3$). (B) The adipogenic phenotypes of 3T3L1 cells transfected with siZfp217 or siCtrl after MDI induction for 6 days were assessed by ORO staining; magnification: $200\times$. 3T3L1 cells were differentiated into adipocytes using MDI cocktail medium. (C) mRNA levels of adipogenic key genes *PPAR γ* , *aP2*, *LPL* and *Adiponectin* at day 6 were detected by QPCR ($n = 3$). (D) Protein levels of *PPAR γ* and *aP2* at day 6 were detected by western blot ($n = 3$). (E) Schematic representation of knockout of *Zfp217*. (F) The adipogenic phenotypes of WT and *Zfp217*^{-/-} cells with the treatment of MDI for 6 days. (G) mRNA levels of *PPAR γ* , *aP2*, *LPL* and *Adiponectin* from WT and *Zfp217*^{-/-} cells with the treatment of MDI for 6 days ($n = 3$). (H) Protein levels of *PPAR γ* and *aP2* from WT and *Zfp217*^{-/-} cells with the treatment of MDI for 6 days ($n = 3$). (I) Protein expression of *Zfp217* in MEF-*Zfp217*^{+/-} cells. (J) The adipogenic phenotypes of MEF-*Zfp217*^{+/-} cells with the treatment of MDI for 6 days. (K) mRNA expression of adipogenic key genes in MEF-*Zfp217*^{+/-} cells with the treatment of MDI for 6 days ($n = 3$). (L) protein expression of adipogenic key genes in MEF-*Zfp217*^{+/-} cells with the treatment of MDI for 6 days ($n = 3$). Presented as means \pm SD (** $P < 0.01$).

1F–H). We also examined the effects of Zfp217 decrease on adipogenesis using the embryonic fibroblasts from mice with haploinsufficiency of *Zfp217* (MEF- *Zfp217*^{+/-}, Figure 1I–L). Overall, our findings suggested that Zfp217 has a profound impact on adipose differentiation.

Zfp217 inhibition enhances m⁶A modification during adipogenesis

Previously, Zfp217 was reported to influence m⁶A modification in embryo stem cells (ESCs) maintenance (8). Here, to screen function of Zfp217 in 3T3L1 cells, we detected m⁶A modification in mRNAs by using dot blot and liquid chromatography-tandem mass spectrometry (LC-MS/MS) quantification. It showed a global increase of m⁶A level in *Zfp217*-depleted cells by using siRNA and CRISPR/Cas9 system, compared with the control group (Figure 2A, B, D and E). m⁶A immunostaining method also revealed higher m⁶A modification in *Zfp217* knockdown cells (Figure 2C). Recently, some papers reported that FTO is a multifunctional demethylase, not only for m⁶A, but also for m⁶Am of mRNA (29). Performed by LC-MS/MS, we also found that m⁶Am level increased significantly in *Zfp217*-deficient

cells (Supplementary Figure S2). It may be noted that the total amount of m⁶A is around 10-fold higher than that of m⁶Am in mRNA, which is consistent with the data mentioned in this paper. Therefore, m⁶A rather than m⁶Am may be main point to focus on here. Moreover, to identify the role of Zfp217 in regulating m⁶A modification during adipogenesis, m⁶A levels were detected by dot blot after 2-day MDI induction. It showed no difference between the control and *Zfp217*-depleted cells, which may imply the early function of Zfp217-m⁶A way in adipogenesis (Figure 2F). m⁶A modification was also dramatically increased in the MEF-*Zfp217*^{+/-} comparing with wild-type (Figure 2G and H). Taken together, these results advised that Zfp217 is critical for cellular m⁶A RNA methylation.

Zfp217 directly activates the transcription of FTO

Although Zfp217 inactivation in cells influenced m⁶A modification, Zfp217 is not a methyltransferase or demethylase *per se*. How does Zfp217 inhibit m⁶A mRNA methylation? To clarify the role of Zfp217 in regulating m⁶A modification, we detected the expression of key proteins involved in m⁶A methylation. Interestingly, knockdown of *Zfp217*

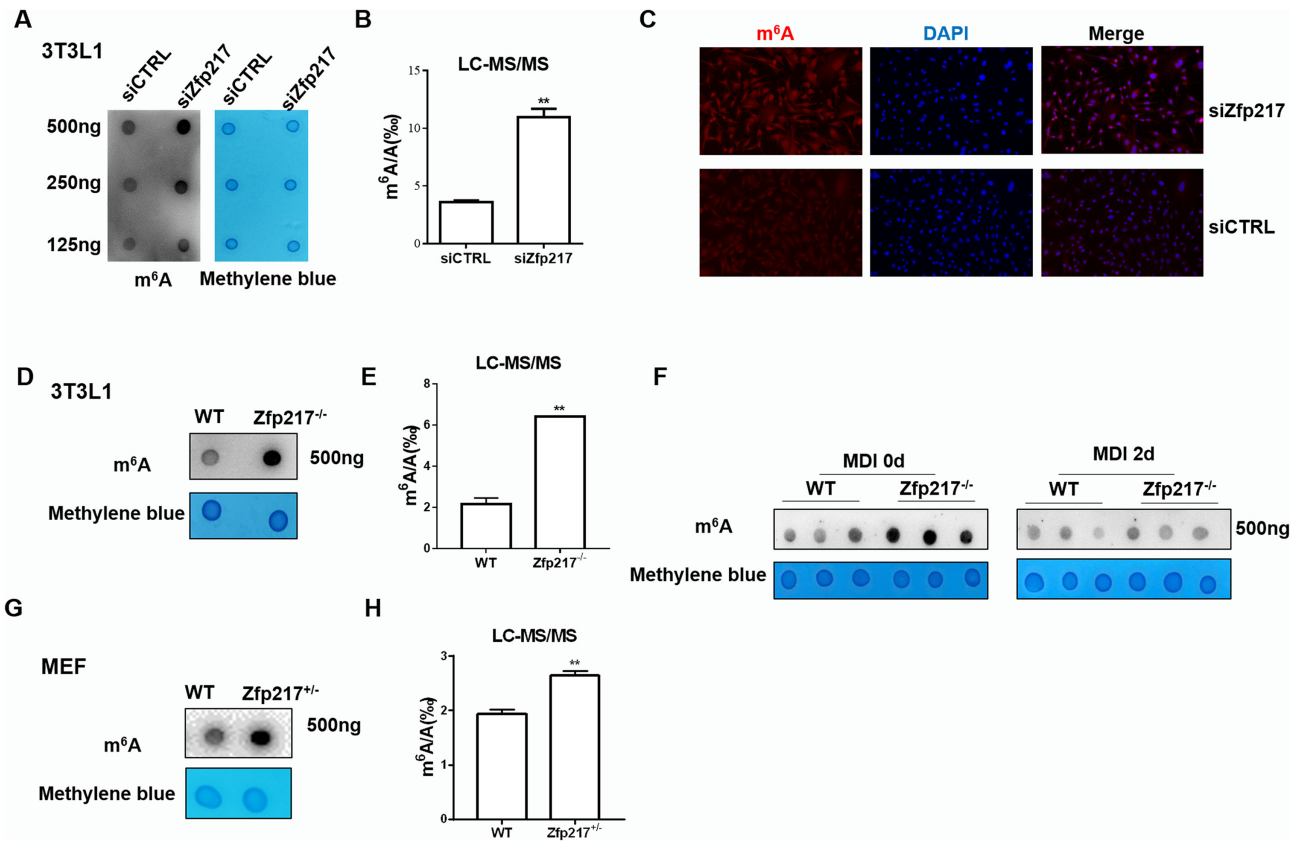


Figure 2. *Zfp217* depletion increases m^6A modification in 3T3L1 cells. (A) Dot blot was used to detect the m^6A modification after knockdown of *Zfp217*. Methylene blue staining was used as a loading control ($n = 3$). (B) m^6A/A ratio in polyadenylated RNA was measured from control and *Zfp217* knockdown 3T3L1 cells using LC-MS/MS ($n = 2$). (C) m^6A immunostaining of 3T3L1 cells transfected with siCtrl and si*Zfp217*. Nucleus was stained with DAPI (magnification: 200 \times). (D) Dot blot was used to detect the m^6A modification after knockout of *Zfp217* ($n = 3$). (E) m^6A modification levels were measured after knockout of *Zfp217* using LC-MS/MS ($n = 2$). (F) m^6A level during adipogenesis of 3T3L1 ($n = 3$). (G) Dot blot was used to detect the m^6A modification in MEF-*Zfp217*^{+/-} cells ($n = 3$). (H) m^6A modification level was measured in MEF-*Zfp217*^{+/-} cells using LC-MS/MS ($n = 2$). Presented as means \pm SD (** $P < 0.01$).

markedly increased the protein expression of METTL3 and decreased the expression of FTO (Figure 3A). We also found that knockdown of *METTL3* increased the protein expression of *Zfp217*, and *METTL3* knockdown rescued the m^6A modification level in *Zfp217* knockdown cells (Supplementary Figure S3A and B). These findings suggested that both FTO and METTL3 may have functions in *Zfp217*-related m^6A modification. Subsequently, mRNA level of *FTO* was coordinately regulated by *Zfp217* overexpression or knockdown in 3T3L1 cells (Figure 3B), whereas *METTL3* level was not changed (Supplementary Figure S3C and D). Henceforth, we refer to verify whether *Zfp217* could regulate the expression of *FTO* as a transcriptional factor.

We reasoned that *FTO* acts as a target gene of *Zfp217* using bioinformatics method (Figure 3C). Next, dual luciferase reporter system was employed to validate that *Zfp217* enhanced the promoter activity of *FTO*, while deletion of the *Zfp217* binding sequence in *FTO* promoter inhibited it (Figure 3C), suggesting a direct regulation of *Zfp217* on *FTO*. Accordingly, localization of *Zfp217* at the promoter region of *FTO* was also confirmed by ChIP-QPCR assays using the *Zfp217* specific antibody with or without MDI treatment (Figure 3D). By gene sequence

analysis, the accurate binding DNA sequence is completely consistent with genomic sequence of *FTO* (Figure 3E). In agreement with these observation, we found that *FTO* rescues the inhibition of adipogenesis with the lack of *Zfp217* and increases the gene expression of *PPAR γ* , *aP2*, *LPL* and *Adiponectin* consistently (Figure 3F and G). Given the rescue of m^6A modification level by *FTO* overexpression (or knockdown) in *Zfp217* knockdown (or overexpressed) 3T3L1 cells, m^6A may be the main target of *Zfp217*-FTO-dependent way to regulate adipogenesis (Figure 3H). Collectively, our data demonstrated that *Zfp217*, act as a transcriptional factor, binds to promoter of *FTO* gene to augment adipogenesis, which may be one way to modulate m^6A modification during adipogenesis.

***Zfp217* positively regulates the epitranscriptome involved in adipogenesis**

To gain an overview of the global role of *Zfp217* in adipogenesis, we performed RNA sequencing (RNA-seq) in control and *Zfp217* knockout 3T3L1 cells with MDI treatment for 0 and 2 d and identified 12 188 and 11 566 different expressed genes (DEG) for 0 and 2d, respectively (Figure 4A; Supplementary Figure S4A and Table S6). Compared with

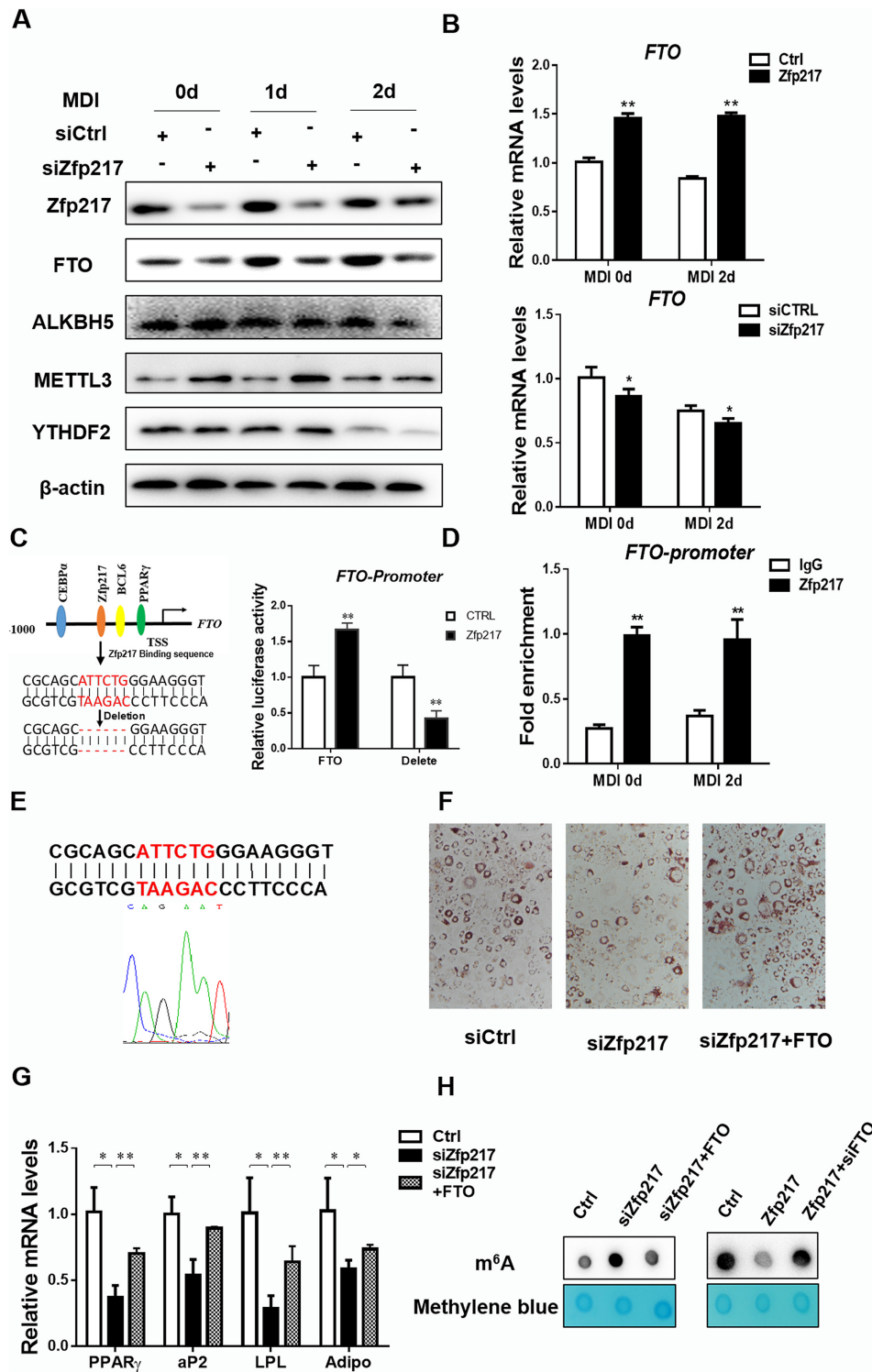


Figure 3. Activation of *FTO* transcription by *Zfp217* for adipogenesis. (A) Protein expression levels of m⁶A-related proteins during MDI treatment in *Zfp217* knockdown cells were detected by western blot ($n = 3$). β -Actin was used as a loading control. (B) mRNA levels of *FTO* in 3T3L1 cells with overexpression and knockdown of *Zfp217* were detected by QPCR ($n = 3$). (C) Left panel: schematic representation of transcription factor binding promoter of *FTO*; right panel: dual-luciferase activity of normal and binding site-deleted *FTO* promoter by overexpressing *Zfp217* in HEK293T cells ($n = 3$). (D) ChIP-QPCR assay was used to measure the binding of *Zfp217* on *FTO* promoter in 3T3L1 cells with or without treatment of MDI ($n = 3$). Total chromatin was indicated as input and IgG was used as a negative control. (E) The position of the amplified regions of *Zfp217* binding sequence in *FTO* promoter was indicated. (F) The effect of *Zfp217* knockdown or together with overexpression of *FTO* on adipogenesis of 3T3L1 cells ($n = 3$). (G) mRNA expression levels of adipogenic genes were measured in 3T3L1 cells with *Zfp217* knockdown or together with overexpression of *FTO* and treated with MDI for 6 days ($n = 3$). (H) The effect of overexpression (or knockdown) of *Zfp217* or together with depletion (or overexpression) of *FTO* in 3T3L1 cells on m⁶A modification ($n = 3$). Presented as means \pm SD (* $P < 0.05$, ** $P < 0.01$).

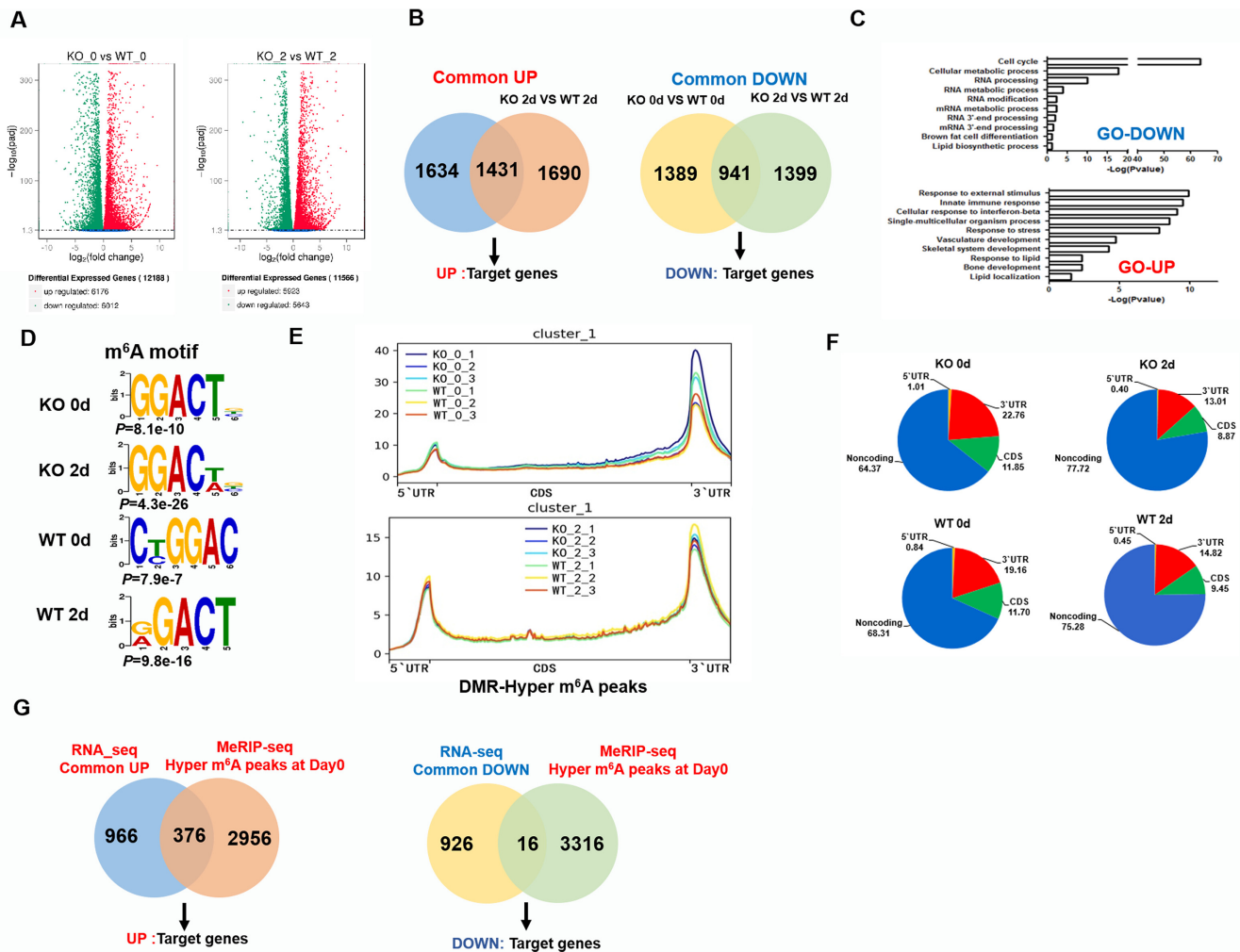


Figure 4. *Zfp217* positively regulates the epitranscriptome of key genes involved in adipogenesis. (A) Overview of different expression genes (DEG) by RNA-seq. (B) Overlapped transcripts of control and *Zfp217* knockout in 3T3L1 cells at 0 or 2 d after MDI treatment by RNA-seq. (C) GO analysis of up- and down-regulated genes by RNA-seq. The P value for the enrichment of biological process GO-term is shown. (D) Sequence logo representing consensus motif of m^6A sites in *Zfp217*-dependent peaks by MeRIP-seq. (E and F) Metagene profiles of m^6A distribution across the transcriptome of 3T3L1 cells at 0 or 2 d after MDI treatment by MeRIP-seq. (G) Overlapped the DEG of RNA-seq with DMR from MDI 0 d of MeRIP-seq respectively to identify the key target genes.

the wild-type, the vast majority (1431) of upregulated genes in *Zfp217* depleted cells with MDI treatment for 0 d notably overlapped with that of the group with MDI for 2 d, while 941 downregulated genes were also identified here (Figure 4B and Supplementary Table S7). By Gene Ontology (GO) analysis, the downregulated genes were found to be mostly associated with cell cycle, RNA processing and lipid biosynthetic progress (Figure 4C; Supplementary Figure S4B; Tables S8 and S9), suggesting that *Zfp217* is involved in proper regulation of RNA processing and lipid metabolism.

Next, to elucidate the mechanism by which *Zfp217* regulates m^6A modification, m^6A methylated RNA immunoprecipitation sequencing (MeRIP-seq) was employed to analyze the m^6A mRNA methylation in control and *Zfp217* knockout 3T3L1 cells with MDI treatment for 0 and 2 d. In agreement with previous reports in mammals, it was found that GGACU is indeed highly enriched and consistently represents as the best sequence motif (Figure 4D).

We next sought to investigate whether critical m^6A sites are affected by *Zfp217* depletion. It revealed that the relative density of m^6A sites in the 5'UTR and 3'UTR are higher than other regions (Figure 4E and F; Supplementary Figure S5A; Table S10). In particularly, *Zfp217* depletion increased the m^6A enrichment after MDI for 0 d, not 2 d, which means these transcripts are in *Zfp217* knockout-dependent manner (Figure 4G). Based on the above results, we assumed that DEG from RNA-seq may be more likely regulated when the m^6A peaks are enriched in these corresponding transcripts of DEG. Thus, we further overlapped the DEG from UP and DOWN groups with 3332 differentially methylated regions (DMRs) from MDI for 0 d group, respectively, to identify the key target genes (Figure 4G; Supplementary Tables S11–S13). Based on RNA-seq data, it was found that cell cycle may be one of the important biological events in *Zfp217* knockout cells. Results of cell cycle and apoptosis, presented by flow cytometry analysis as well

as mRNA expression of key genes, suggested that knockout of *Zfp217* may suppress proliferation and promote apoptosis of 3T3L1 cell with or without MDI treatment (Supplementary Figure S6). However, cell cycle related key genes cannot be found in MeRIP-seq data overlapped with RNA-seq data, which might suggest that cell cycle is not the main related biological event in *Zfp217*-m⁶A mediated adipogenesis.

Some of other key targets were selected for further experiments, *Ccdc141* from UP group, *Efcab11* from DOWN group, *Hspa1a* from references and observed significant changes in RNA-seq data (Supplementary Figure S4C). Next, to validate the results of RNA-seq and MeRIP-seq, these genes were chosen for QPCR and MeRIP-QPCR analysis. They showed similar gene expression profiles with RNA-seq (Figure 5A and Supplementary Figure S4C), and MeRIP-QPCR revealed an increase of m⁶A modification at these transcripts after *Zfp217* depletion (Figure 5B; Supplementary Figure S5B and C). Moreover, to validate the roles of these target genes, loss-of-function assays by siRNAs for *Ccdc141*, *Hspa1a* and *Efcab11* exhibited decreased levels of adipogenesis (Figure 5C–E). Taken together, our data revealed the positive relationship between mRNA expression and m⁶A mRNA methylation upon *Zfp217* knockout during adipogenesis.

***Zfp217* interacts with YTHDF2 to maintain m⁶A demethylation activity of FTO**

Previous study reported *Zfp217* exerts its function through interacting with other proteins in embryonic development and human tumors (22). To further explore the global molecular mechanism by which *Zfp217* promotes adipogenesis, we performed immunoprecipitation experiments with overexpression of Flag-N-*Zfp217* in HEK293T cells followed by immunoblotting proteins related to m⁶A mRNA modification (Supplementary Figure S7A). Unexpectedly, FTO, ALKBH5 or METTL3/14 were not detected by Co-IP with Flag antibody (Supplementary Figure S7A). Using antibodies against METTL3 and *Zfp217*, endogenous METTL3 and *Zfp217* interaction may be found in HEK293T cells (Supplementary Figure S7B), which is similar to the results in ESCs (8). Strikingly, we verified a specific interaction between *Zfp217* and YTHDF2 by Co-IP and reverse Co-IP experiments of the endogenous proteins as well as Flag-tagged proteins both in 3T3L1 (with or without MDI treatment) and HEK293T cells (Figure 6A and Supplementary Figure S7C). Notably, *Zfp217*-YTHDF2 interaction was RNA-independent (Supplementary Figure S7D) as treating the cellular extracts with RNase A does not affect the precipitation of YTHDF2. To further confirm the subcellular interaction, fractions isolated from nucleus and cytoplasm were used to measure the expression of *Zfp217* and YTHDF2. Consequently, both of these two proteins were whole cell distributed both in 3T3L1 and HEK293T. Intriguingly, *Zfp217* has more expression in cytoplasm than nucleus (Figure 6B and Supplementary Figure S7E). Moreover, we also performed confocal microscopy for monitoring the cellular location of endogenous *Zfp217* and YTHDF2. Interestingly, co-localization of YTHDF2 and *Zfp217* was observed in nucleus and cytoplasm using con-

focal Z-analysis, which may indicate the specific function of YTHDF2 in *Zfp217*-dependent adipogenesis (Figure 6C and D; Supplementary Figure S7F).

As reported that YTHDF2 could maintain m⁶A level by inhibiting FTO activity under heat stress (16), we further comprehensively analyzed biological function of interaction between YTHDF2 and *Zfp217* to FTO. As expected, overexpression of *FTO* and *Zfp217* showed lower m⁶A level and YTHDF2 blocked the demethylase activity of FTO to increase m⁶A levels, whereas *Zfp217* functioned as a regulator to tilt the equilibrium toward demethylation (Figure 7A and Supplementary Figure S8A). Furthermore, we confirmed direct competition between FTO and YTHDF2 to target m⁶A ssRNA from *Hspa1a* (16) by *in vitro* m⁶A RNA pull-down assay (Figure 7B and D). Obviously, *Zfp217*, not binding to RNA, interfered with location of YTHDF2 (Figure 7C) and rescued FTO to bind RNA (Figure 7D). Combining *in vitro* RNA pull-down and dot blot assay to assess the m⁶A demethylation activity of FTO, it was also confirmed that *Zfp217* sequestered YTHDF2 to maintain m⁶A demethylation activity of FTO (Figure 7E). To determine whether *Zfp217* directly interacts with YTHDF2 *in vitro*, we performed LSPR. The results clearly showed that *Zfp217* directly interacts with YTHDF2 in a dose-dependent manner (Figure 7C). After combining YTHDF2, *Zfp217* prohibited m⁶A-containing ssRNA from binding with YTHDF2 (Figure 7D). Overall, our findings indicated that *Zfp217* interacts with YTHDF2 to keep the accessibility of FTO to m⁶A sites.

Knockdown of YTHDF2 rescues inhibition of *Zfp217* depletion-mediated adipogenesis

To further investigate the underlying molecular mechanism how *Zfp217* regulates the target genes by m⁶A modification, we focused on YTHDF2 and verified its role in *Zfp217*-mediated adipogenesis. Intriguingly, knockdown of YTHDF2 drastically rescued adipogenesis in *Zfp217*-deficient cells (Figure 8A and B), while the m⁶A modification of genes was lower after YTHDF2 knockdown (Figure 8C), suggesting the critical role of YTHDF2 in *Zfp217*-mediated adipogenesis.

Collectively, these results identified that *Zfp217* balances the expression of key genes in a YTHDF2-dependent way, ultimately leading to the promotion of adipogenesis. We proposed a model in which *Zfp217* regulates adipogenesis in Figure 9.

DISCUSSION

Adipogenesis involves different levels of regulatory mechanism, with the majority of known control factors are involved in transcriptional regulation (35). In the present study, we delineated a role for multifunctional factor *Zfp217* in adipocyte differentiation. Complementary *in vitro* and *ex vivo* analyses demonstrated that depletion of *Zfp217* inhibits adipogenic protein PPAR γ and other key adipogenic-related protein expression and in turn adipogenesis (Figure 1). Interestingly, deletion of *Zfp217* increases global m⁶A RNA modification, which indicates the role of *Zfp217* at post-transcriptional level (Figures 2 and 4). Mechanis-

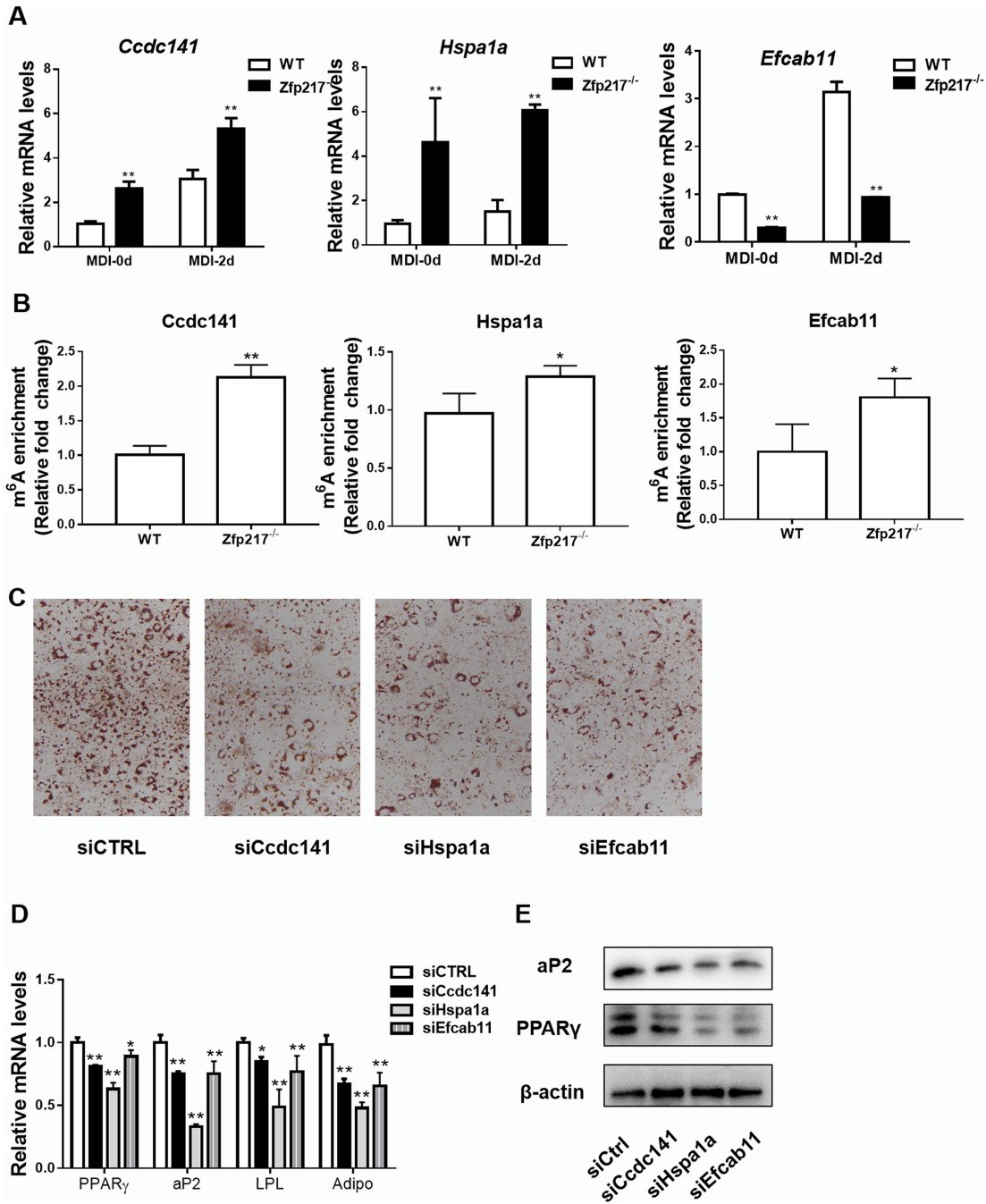


Figure 5. Effect of *Zfp217* deletion on the expression of target genes. (A) Validation of *Ccdc141*, *Hspa1a* and *Efcab11* mRNA levels from RNA-seq data by QPCR ($n = 3$). (B) Validation of m⁶A modification in *Ccdc141*, *Hspa1a* and *Efcab11* mRNA by MeRIP-QPCR ($n = 3$). (C) The adipogenic phenotypes of 3T3L1 cells transfected with *siCcdc141*, *siHspa1a*, *siEfcab11* or *siCtrl* after MDI induction for 6 days were assessed by ORO staining. (D) mRNA expression levels of adipogenic key genes *PPAR γ* , *aP2*, *LPL* and *Adiponectin* were detected by QPCR ($n = 3$). (E) Protein levels of *PPAR γ* and *aP2* were detected by western blot ($n = 3$). Presented as means \pm SD (* $P < 0.05$, ** $P < 0.01$).

tically, we showed that *Zfp217* binds directly to the promoter of m⁶A demethylase *FTO* (Figure 3C–E), and interacts with m⁶A reader *YTHDF2* (Figure 6), thereby enhances the location and demethylase activity of *FTO* to m⁶A target RNAs (Figure 7). Ultimately, *Zfp217* promotes adipogenesis in an m⁶A-*YTHDF2*-dependent manner (Figure 8). These findings for the first time demonstrated the

multifaceted and complex function of *Zfp217* in adipogenesis.

Zfp217* acts as a classical transcription factor to promote expression of *FTO

Zfp217 is a classical transcriptional factor from zinc finger protein family, with eight conserved C₂H₂ zinc finger mo-

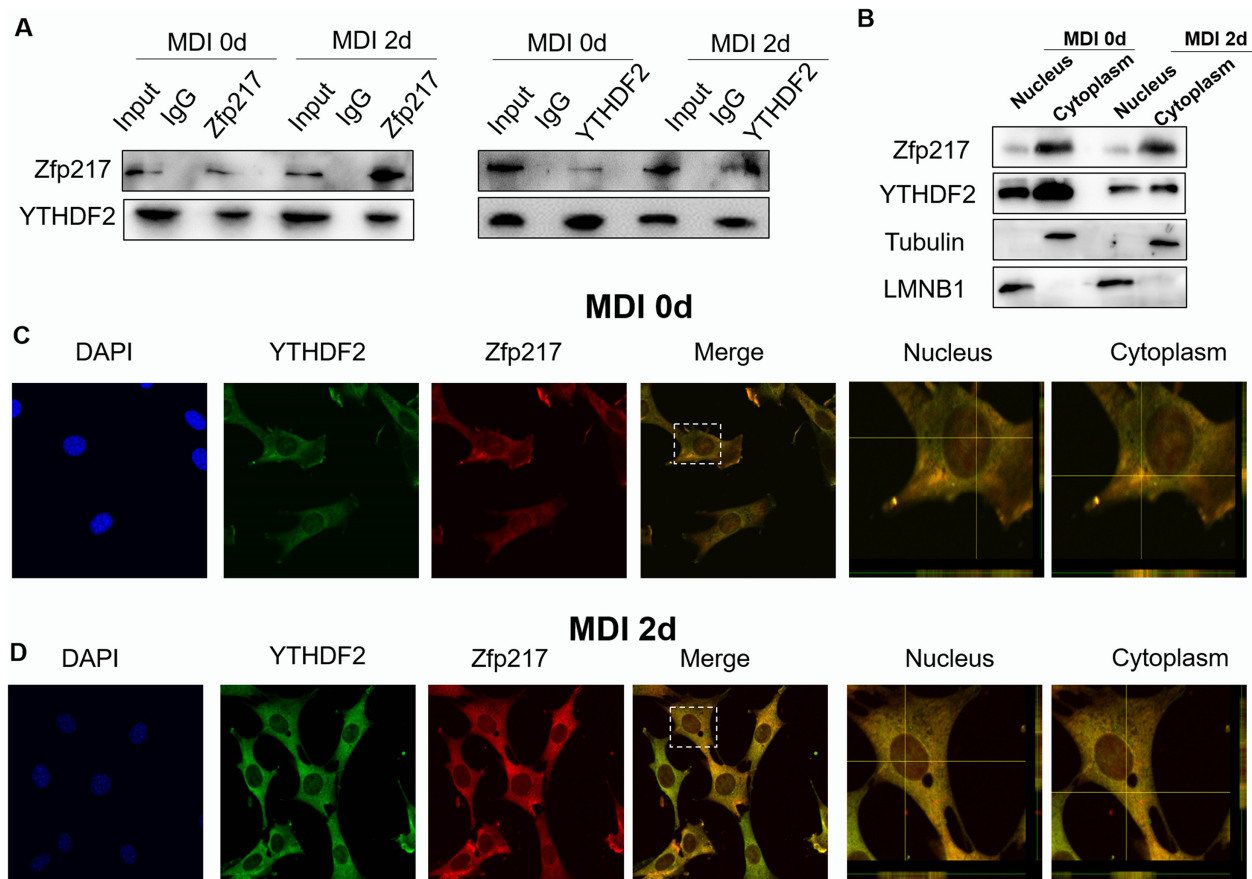


Figure 6. Zfp217 interacts with YTHDF2. (A) CoIP and reverse CoIP analysis of interaction between Zfp217 and YTHDF2 in 3T3L1 cells with or without MDI treatment for 2 days using antibodies against the endogenous proteins ($n = 3$). IgG was used as a negative control. (B) Protein expression level of Zfp217 and YTHDF2 in cytoplasmic and nuclear fractions was analyzed by western blot ($n = 3$). (C and D) Subcellular localization of Zfp217 and YTHDF2 in 3T3L1 cells with or without MDI treatment for 2 days. 3T3L1 cells were immunostained with antibodies against Zfp217 and YTHDF2. DAPI was used for nuclear staining. Cells analyzed with a confocal laser scanning microscope (63 \times magnification) with Z-scan analysis.

tifs and a proline-rich transactivation domain (18). Conceptually, after binding to a specific DNA sequence of target gene, Zfp217 exerts activation of specific gene expression programs, and also cooperates in transcriptional silencing programs by recruiting chromatin modifiers in embryonic development and human tumors (17,21,22). Thus, depletion of Zfp217 may directly affect the expression of downstream target genes. As reported by our group previously, expression of Zfp217 was found to be significantly up-regulated during adipogenesis (24). Accordingly, in current study, we showed that deletion of Zfp217 in 3T3L1 cells significantly blocks the expression of *PPAR γ* , *aP2* and other adipogenic genes by performing RNA-seq together with the adipogenic phenotype (Figures 1 and 4A–C), which indicates that Zfp217 might take part in transcriptional cascade regulation of key genes in adipogenesis.

Using bioinformatics of promoter binding analysis, we predicted that *FTO* is the potential target gene of Zfp217 (Figure 3C–E). Interestingly, *FTO* is well known for its role in associated with obesity and related diseases (11,36). The numbers of studies have been reported the positive function of *FTO* in adipogenesis (9,15). Here, the multiple methods for transcriptional regulation validated that Zfp217 directly binds to the promoter of *FTO*, and overexpression

of *FTO* reversed inhibition of adipogenesis with Zfp217 knockdown (Figure 3F and G), thereby providing a reliable cue for clarifying the facilitative role of Zfp217 in adipogenesis.

Zfp217 mediates m⁶A mRNA methylation through FTO and YTHDF2

Previous studies showed that Zfp217 sustains undifferentiated state of ESCs and supports its pluripotent state by epigenetically regulating m⁶A methylation (8). In this study, we found that Zfp217 depletion significantly increases the m⁶A modification level in 3T3L1 cells and MEF-Zfp217^{+/-} (Figure 2), but it needs to be unraveled how could a transcription factor regulate m⁶A modification.

FTO was reported as the first m⁶A demethylase of mRNA, and the function of *FTO* in adipogenesis has been linked to its m⁶A demethylase activity (13,36). Here, we showed knockdown of *FTO* retrieved m⁶A modification level in Zfp217 overexpressed cells (Figure 3H). The finding indicated that Zfp217 reduces m⁶A modification through increasing the expression of *FTO* in a transcriptional regulatory way. Consistently, other studies have also reported that with the treatment of R-2HG, CEBP α suppresses the

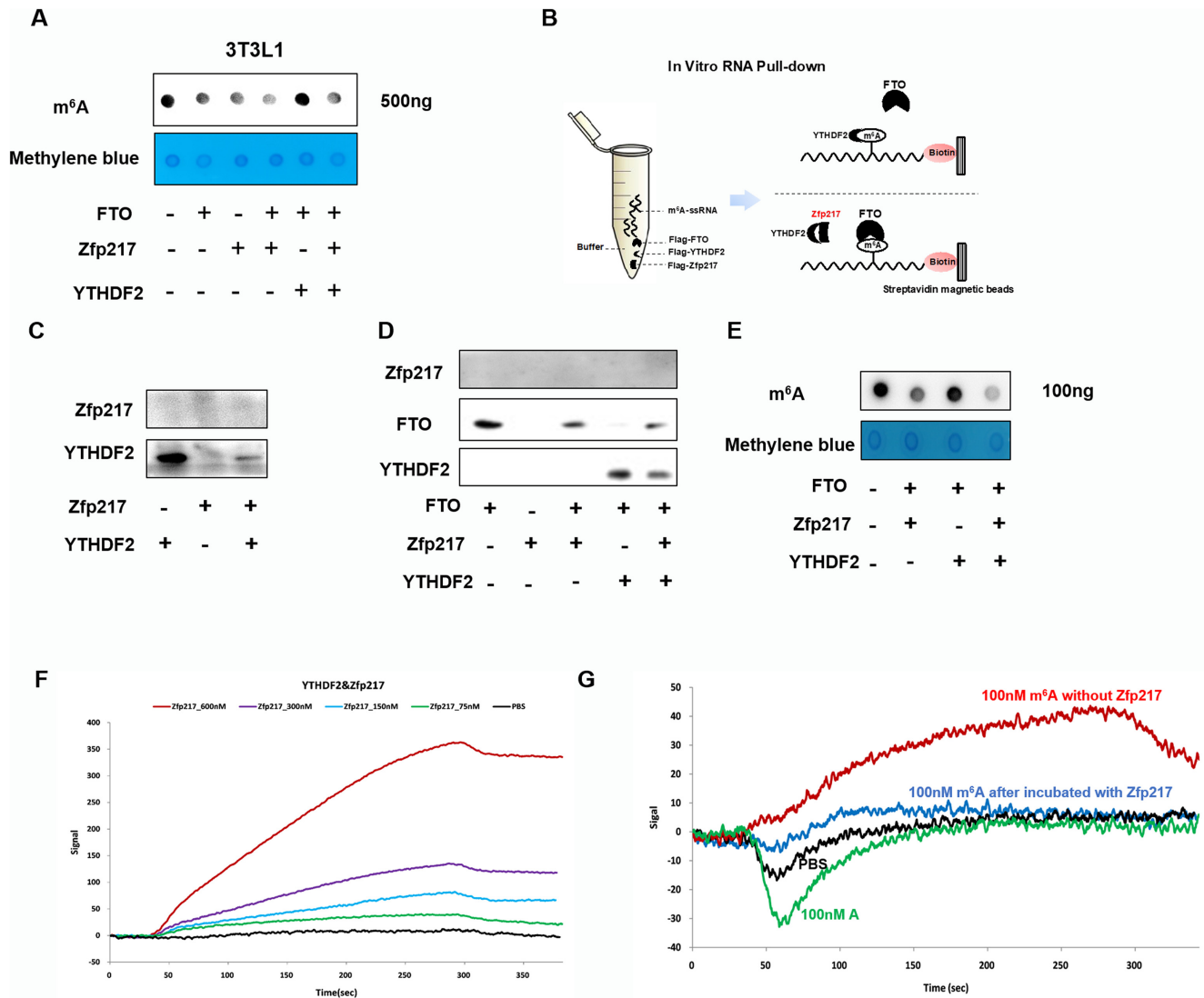


Figure 7. Zfp217 influences competition between YTHDF2 and FTO in m⁶A-binding sites. (A) Dot blot was used to measure the effect of overexpression of FTO, Zfp217 or YTHDF2 in 3T3L1 cells on m⁶A modification (*n* = 3). (B) Schematic representation of RNA pull down. (C) Synthesized mRNA with m⁶A was incubated with YTHDF2 in the absence or presence of Zfp217, followed by RNA pull-down and western blot (*n* = 3). (D) Synthesized mRNA with m⁶A was incubated with FTO in the absence or presence of YTHDF2 and Zfp217, followed by RNA pull-down and western blot (*n* = 3). (E) mRNA of 3T3L1 cells was incubated with FTO, Zfp217 and YTHDF2, followed by m⁶A dot blot (*n* = 3). (F) Zfp217 directly interacts with YTHDF2 in a dose-dependent manner by LSPR. (G) Zfp217 blocked the binding capacity between YTHDF2 and m⁶A ssRNA by LSPR.

expression of FTO by directly binding to its promoter, resulting to the high m⁶A modification (32). Interestingly, it was observed high m⁶A modification of *FTO* mRNA itself after *Zfp217* knockout through MeRIP-seq as well, implying a feedback mechanism of which high m⁶A modification of *FTO* mRNA inhibits FTO expression itself (32). We also found a higher m⁶A modification in *FTO* mRNA in *Zfp217* deficiency cells (Supplementary Figure S5C). And, strikingly, we have previously reported that higher m⁶A modification in *FTO* mRNA leads to its low protein expression in placenta (27). Together, it may be certain to infer that the transcriptional activation of *FTO* by *Zfp217* in m⁶A modification acts as an inherent property of this transcriptional factor.

Notably, Zfp217 is also known as a core component of protein complexes with histone deacetylase (HDAC), CoREST and CTBPs (37–39), which suggests its multi-functional roles in biology events. Therefore, clarifying the interacted proteins of Zfp217 could gain insight into the molecular mechanism of Zfp217-dependent adipogenesis. Here, we focused on the m⁶A-related proteins that may be interacted with Zfp217. Applied Co-IP with antibodies against endogenous proteins, we found the interaction between METTL3 and Zfp217 (Supplementary Figure S7B), which corroborated the previous study in HEK293T cells (8). Interestingly, there may be mutual inhibition between METTL3 and Zfp217 and *METTL3* knockdown rescued the m⁶A modification level in *Zfp217* knockdown cells (Fig-

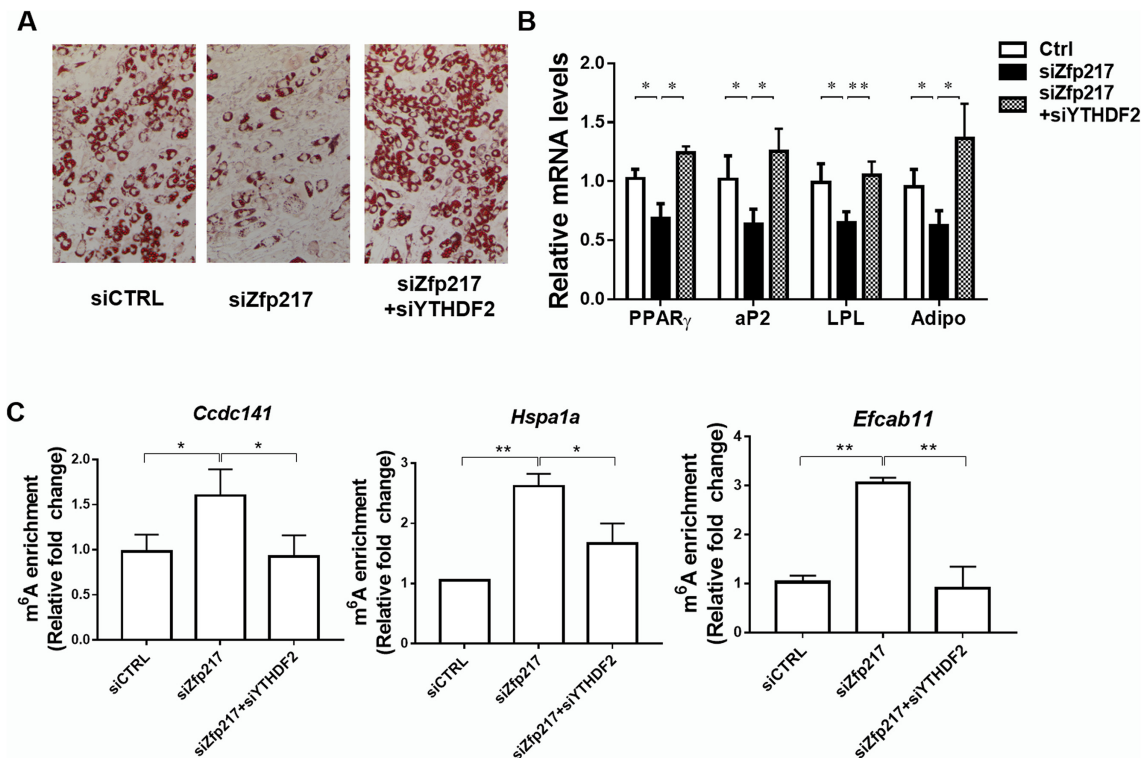


Figure 8. Knockdown of *YTHDF2* rescues inhibition of *Zfp217* depletion-mediated adipogenesis. (A) Knockdown of *YTHDF2* rescues adipogenesis in *Zfp217*-deficient 3T3L1 cells. The adipogenic phenotypes were assessed by ORO staining; magnification: 200 \times . (B) mRNA levels of adipogenic key genes were detected by QPCR ($n = 3$). (C) MeRIP-QPCR was performed to detect the m⁶A abundance of target genes in *YTHDF2* knockdown cells ($n = 3$).

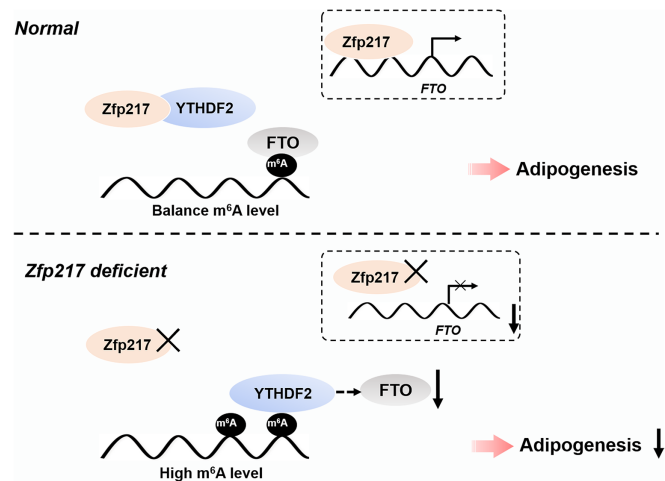


Figure 9. A diagram demonstrates the role of *Zfp217*-dependent m⁶A modification in adipogenesis. In our model, *Zfp217* orchestrates *FTO* expression at transcriptional level and interaction with *YTHDF2* to regulate m⁶A mRNA methylation and facilitates adipogenic differentiation in a *YTHDF2*-dependent manner.

ure 3A; Supplementary Figure S3A and B), suggesting it may be one of the well-known ways to regulate m⁶A modification (8). We also validated the actual interaction between *Zfp217* and m⁶A 'reader' protein *YTHDF2* (Figure 6). Monitored by confocal microscope, the interaction

between *Zfp217* and *YTHDF2* occurred almost in whole cell and mainly in cytoplasm after MDI for 2 days. As in earlier study, it has elucidated that *YTHDF2* preserves m⁶A methylation by limiting *FTO* from demethylation under heat shock stress (16). Here, we found that *Zfp217* may act as a regulator for *YTHDF2*-*FTO* competition, which sequesters *YTHDF2* from limiting the accessibility of *FTO* to m⁶A sites (Figure 7). Overall, besides transcriptional activation of *FTO*, it seems that *Zfp217* could sustain the demethylase activity of *FTO* by interaction with m⁶A 'reader' *YTHDF2*. Of particular note, a recent seminal study revealed a crosstalk between histone modification and RNA methylation and uncovered another layer of gene expression regulation (40). Here, *Zfp217* may also function across transcriptional and post-transcriptional level, which sheds new light on the role of this transcription factor in adipogenesis (22).

In summary, we illustrated that *Zfp217* is essential for adipogenesis by connecting gene transcription with m⁶A mRNA modification. The regulatory role of *Zfp217* that keeps low m⁶A modification of the target mRNAs provides fundamental insight into the post-transcriptional gene regulation network in adipocyte differentiation, revealing potential novel ways to regulate adipogenesis and other vital events at this new frontier of transcriptional factors. These findings offer a new approach to dissect the molecular mechanism of adipogenesis, and, ultimately, counteract obesity and its associated risks of metabolic syndromes.

DATA AVAILABILITY

The accession number for the next-generation sequencing data reported in this paper is NCBI GEO: GSE119564.

SUPPLEMENTARY DATA

Supplementary Data are available at NAR Online.

ACKNOWLEDGEMENTS

We thank Dr Guifang Jia (Peking University, China) and Dr Chuan He (The University of Chicago, USA) for pure m⁶Am nucleoside; Dr Bifeng Yuan (Wuhan University, China) for detailed advices about LC-MS/MS; Dr Shengqing Li and Qiongyao Gu for helping with LC-MS/MS analysis.

FUNDING

National Natural Science Foundation of China [31472075]; China Agriculture Research System [CARS-36]; Hubei provincial Creative TeamProject of Agricultural Science and Technology (2007-620); Fundamental Research Funds for the Central Universities of China [2662017PY017]. Funding for open access charge: National Natural Science Foundation of China [31472075].

Conflict of interest statement. None declared.

REFERENCES

- Rosen, E.D. and Spiegelman, B.M. (2014) What we talk about when we talk about fat. *Cell*, **156**, 20–44.
- Siersbæk, R., Nielsen, R. and Mandrup, S. (2012) Transcriptional networks and chromatin remodeling controlling adipogenesis. *Trends Endocrinol. Metab. Tem.*, **23**, 56–64.
- Roundtree, I.A., Evans, M.E., Pan, T. and He, C. (2017) Dynamic RNA modifications in gene expression regulation. *Cell*, **169**, 1187–1200.
- Meyer, K.D. and Jaffrey, S.R. (2014) The dynamic epitranscriptome: N⁶-methyladenosine and gene expression control. *Nat. Rev. Mol. Cell Biol.*, **15**, 313–326.
- Zhao, B.S., Roundtree, I.A. and He, C. (2017) Post-transcriptional gene regulation by mRNA modifications. *Nat. Rev. Mol. Cell Biol.*, **18**, 31–42.
- Wang, X., Lu, Z., Gomez, A., Hon, G.C., Yue, Y., Han, D., Fu, Y., Parisien, M., Dai, Q. and Jia, G. (2014) N⁶-methyladenosine-dependent regulation of messenger RNA stability. *Nature*, **505**, 117–120.
- Geula, S., Moshitchmoshkovitz, S., Dan, D., Mansour, A.F., Kol, N., Salmonddivon, M., Hershkovitz, V., Peer, E., Mor, N. and Manor, Y.S. (2015) m⁶A mRNA methylation facilitates resolution of naive pluripotency toward differentiation. *Science*, **6225**, 1002–1006.
- Aguilo, F., Zhang, F., Sancho, A., Fidalgo, M., Di Cecilia, S., Vashisht, A., Lee, D.F., Chen, C.H., Rengasamy, M., Andino, B. et al. (2015) Coordination of m⁶A mRNA methylation and gene transcription by ZFP217 regulates pluripotency and reprogramming. *Cell Stem Cell*, **17**, 689–704.
- Wang, X., Zhu, L., Chen, J. and Wang, Y. (2015) mRNA m⁶A methylation downregulates adipogenesis in porcine adipocytes. *Biochem. Biophys. Res. Commun.*, **459**, 201–207.
- Kobayashi, M., Ohsugi, M., Sasako, T., Awazawa, M., Umehara, T., Iwane, A., Kobayashi, N., Okazaki, Y., Kubota, N., Suzuki, R. et al. (2018) The RNA methyltransferase complex of WTAP, METTL3, and METTL14 regulates mitotic clonal expansion in adipogenesis. *Mol. Cell Biol.*, **38**, e00116-18.
- Dina, C., Meyre, D., Gallina, S., Durand, E., Körner, A., Jacobson, P., Carlsson, L.M., Kiess, W., Vatin, V. and Lecoq, C. (2007) Variation in FTO contributes to childhood obesity and severe adult obesity. *Nat. Genet.*, **39**, 724–726.
- Loos, R.J. and Yeo, G.S. (2014) The bigger picture of FTO: the first GWAS-identified obesity gene. *Nat. Rev. Endocrinol.*, **10**, 51–61.
- Zhao, X., Yang, Y., Sun, B.F., Shi, Y., Yang, X., Xiao, W., Hao, Y.J., Ping, X.L., Chen, Y.S. and Wang, W.J. (2014) FTO-dependent demethylation of N⁶-methyladenosine regulates mRNA splicing and is required for adipogenesis. *Cell Res.*, **24**, 1403–1419.
- Wu, R., Yao, Y., Jiang, Q., Cai, M., Liu, Q., Wang, Y. and Wang, X. (2018) Epigallocatechin gallate targets FTO and inhibits adipogenesis in an mRNA m⁶A-YTHDF2-dependent manner. *Int. J. Obes.*, **42**, 1378–1388.
- Merkstein, M., Laber, S., McMurray, F., Andrew, D., Sachse, G., Sanderson, J., Li, M., Usher, S., Sellayah, D. and Ashcroft, F.M. (2015) FTO influences adipogenesis by regulating mitotic clonal expansion. *Nat. Commun.*, **6**, 6792.
- Zhou, J., Wan, J., Gao, X., Zhang, X., Jaffrey, S.R. and Qian, S.B. (2015) Dynamic m⁶A mRNA methylation directs translational control of heat shock response. *Nature*, **526**, 591–594.
- Rahman, M.T., Nakayama, K., Rahman, M., Nakayama, N., Ishikawa, M., Katagiri, A., Iida, K., Nakayama, S., Otsuki, Y., Shih, Ie, M. et al. (2012) Prognostic and therapeutic impact of the chromosome 20q13.2 ZNF217 locus amplification in ovarian clear cell carcinoma. *Cancer*, **118**, 2846–2857.
- Quinlan, K.G., Verger, A., Yaswen, P. and Crossley, M. (2007) Amplification of zinc finger gene 217 (ZNF217) and cancer: when good fingers go bad. *Biochim. Biophys. Acta*, **1775**, 333–340.
- Rooney, P.H., Boonsong, A., Mcfadyen, M.C., Mcleod, H.L., Cassidy, J., Curran, S. and Murray, G.I. (2004) The candidate oncogene ZNF217 is frequently amplified in colon cancer. *J. Pathol.*, **204**, 282–288.
- Lin, Y., Li, X.Y., Willis, A.L., Liu, C., Chen, G. and Weiss, S.J. (2014) Snail1-dependent control of embryonic stem cell pluripotency and lineage commitment. *Nat. Commun.*, **5**, 3070.
- Kwak, S., Kim, T.W., Kang, B.H., Kim, J.H., Lee, J.S., Lee, H.T., Hwang, I.Y., Shin, J., Lee, J.H. and Cho, E.J. (2018) Zinc finger proteins orchestrate active gene silencing during embryonic stem cell differentiation. *Nucleic Acids Res.*, **46**, 6592–6607.
- Lee, D.F., Walsh, M.J. and Aguilo, F. (2016) ZNF217/ZFP217 meets chromatin and RNA. *Trends Biochem. Sci.*, **41**, 986–988.
- Xiang, H., Zhong, Z.X., Peng, Y.D. and Jiang, S.W. (2017) The emerging role of Zfp217 in adipogenesis. *Int. J. Mol. Sci.*, **18**, 1367.
- Jiang, S., Wei, H., Song, T., Yang, Y., Peng, J. and Jiang, S. (2013) Transcriptome comparison between porcine subcutaneous and intramuscular stromal vascular cells during adipogenic differentiation. *PLoS One*, **8**, e77094.
- Xu, F., Gao, Z., Zhang, J., Rivera, C.A., Yin, J., Weng, J. and Ye, J. (2010) Lack of SIRT1 (Mammalian Sirtuin 1) activity leads to liver steatosis in the SIRT1^{+/−} mice: a role of lipid mobilization and inflammation. *Endocrinology*, **151**, 2504–2514.
- Song, T., Zhou, Y., Peng, J., Tao, Y.X., Yang, Y., Xu, T., Peng, J., Ren, J., Xiang, Q. and Wei, H. (2016) GPR120 promotes adipogenesis through intracellular calcium and extracellular signal-regulated kinase 1/2 signal pathway. *Mol. Cell Endocrinol.*, **434**, 1–13.
- Song, T., Lu, J., Deng, Z., Xu, T., Yang, Y., Wei, H., Li, S., Jiang, S. and Peng, J. (2018) Maternal obesity aggravates the abnormality of porcine placenta by increasing N⁶-methyladenosine. *Int. J. Obes.*, **42**, 1812–1820.
- Jia, G., Fu, Y., Zhao, X., Dai, Q., Zheng, G., Yang, Y., Yi, C., Lindahl, T., Pan, T. and Yang, Y.G. (2011) N⁶-Methyladenosine in nuclear RNA is a major substrate of the obesity-associated FTO. *Nat. Chem. Biol.*, **7**, 885–887.
- Wei, J., Liu, F., Lu, Z., Fei, Q., Ai, Y., He, P.C., Shi, H., Cui, X., Su, R., Klungland, A. et al. (2018) Differential m⁶A, m⁶Am, and m¹A demethylation mediated by FTO in the cell nucleus and cytoplasm. *Mol. Cell*, **71**, 973–985.
- Zhang, C., Samanta, D., Lu, H., Bullen, J.W., Zhang, H., Chen, I., He, X. and Semenza, G.L. (2016) Hypoxia induces the breast cancer stem cell phenotype by HIF-dependent and ALKBH5-mediated m⁶A-demethylation of NANOG mRNA. *Proc. Natl. Acad. Sci. U.S.A.*, **113**, E2047.
- Dominissini, D., Moshitch-Moshkovitz, S., Salmon-Divon, M., Amariglio, N. and Rechavi, G. (2013) Transcriptome-wide mapping of N⁶-methyladenosine by m⁶A-seq based on immunocapturing and massively parallel sequencing. *Nat. Protoc.*, **8**, 176–189.

32. Su,R., Dong,L., Li,C., Nachtergaele,S., Wunderlich,M., Qing,Y., Deng,X., Wang,Y., Weng,X. and Hu,C. (2017) R-2HG exhibits Anti-tumor activity by targeting FTO/m6A/MYC/CEBPA signaling. *Cell*, **172**, 90–105.
33. Panneer,S.S., Roth,B.M., Nganga,R., Kim,J., Cooley,M.A., Helke,K., Smith,C.D. and Ogretmen,B. (2018) Balance between senescence and apoptosis is regulated by telomere damage-induced association between p16 and caspase-3. *J. Biol. Chem.*, **293**, 9784–9800.
34. McGurn,L.D., Moazami-Goudarzi,M., White,S.A., Suwal,T., Brar,B., Tang,J.Q., Espie,G.S. and Kimber,M.S. (2016) The structure, kinetics and interactions of the β -carboxysomal β -carbonic anhydrase, CcaA. *Biochem. J.*, **473**, 4559–4572.
35. Rosen,E.D. and Macdougald,O.A. (2006) Adipocyte differentiation from the inside out. *Nat. Rev. Mol. Cell Biol.*, **7**, 885–896.
36. Deng,X., Su,R., Stanford,S. and Chen,J. (2018) Critical enzymatic functions of FTO in obesity and cancer. *Front. Endocrinol.*, **9**, 396.
37. Cowger,J.J.M., Zhao,Q., Isovich,M. and Torchia,J. (2007) Biochemical characterization of the zinc-finger protein 217 transcriptional repressor complex: identification of a ZNF217 consensus recognition sequence. *Oncogene*, **26**, 3378–3386.
38. Quinlan,K.G.R., Nardini,M., Verger,A., Francescato,P., Yaswen,P., Corda,D., Bolognesi,M. and Crossley,M. (2006) Specific recognition of ZNF217 and other zinc finger proteins at a surface groove of C-Terminal binding proteins. *Mol. Cell. Biol.*, **26**, 8159–8172.
39. Banck,M.S., Li,S., Nishio,H., Cheng,W., Beutler,A.S. and Walsh,M.J. (2009) The ZNF217 oncogene is a candidate organizer of repressive histone modifiers. *Epigenetics*, **4**, 100–106.
40. Huang,H., Weng,H., Zhou,K., Wu,T., Zhao,B.S., Sun,M., Chen,Z., Deng,X., Xiao,G. and Auer,F. (2019) Histone H3 trimethylation at lysine 36 guides m⁶A RNA modification co-transcriptionally. *Nature*, **567**, 414–419.